Neutrinoless double-β decay in the neutrino-extended standard model

Wouter Dekens,[1,*] Jordy de Vries,[2,3,†] Emanuele Mereghetti,[4,‡] Javier Menéndez,[5,6,§] Pablo Soriano,[5,6,‖] and Guanghui Zhou[7,2,3,¶]

[1]*Institute for Nuclear Theory, University of Washington, Seattle, Washington 98195-1550, USA*
[2]*Institute for Theoretical Physics Amsterdam and Delta Institute for Theoretical Physics, University of Amsterdam, Science Park 904, 1098 XH Amsterdam, The Netherlands*
[3]*Nikhef, Theory Group, Science Park 105, 1098 XG Amsterdam, The Netherlands*
[4]*Los Alamos National Laboratory, Theoretical Division T-2, Los Alamos, New Mexico 87545, USA*
[5]*Departament de Física Quàntica i Astrofísica, Universitat de Barcelona 08028, Spain*
[6]*Institut de Ciències del Cosmos, Universitat de Barcelona 08028, Spain*
[7]*CAS Key Laboratory of Theoretical Physics, Institute of Theoretical Physics, Chinese Academy of Sciences, Beijing 100190, People's Republic of China*

(Received 20 March 2023; revised 13 September 2023; accepted 18 September 2023; published 9 October 2023)

We investigate neutrinoless double-beta decay ($0\nu\beta\beta$) in the minimal extension of the standard model of particle physics, the νSM, where gauge-singlet right-handed neutrinos give rise to Dirac and Majorana neutrino mass terms. We focus on the associated sterile neutrinos and argue that the usual evaluation of their contributions to $0\nu\beta\beta$, based on mass-dependent nuclear matrix elements, is missing important contributions from neutrinos with ultrasoft and hard momenta. We identify the hadronic and nuclear matrix elements that enter the new contributions, and calculate all relevant nuclear matrix elements for ^{136}Xe using the nuclear shell model. Finally, we illustrate the impact on $0\nu\beta\beta$ rates in specific neutrino mass models and show that the new contributions significantly alter the $0\nu\beta\beta$ rate in most parts of the νSM parameter space.

DOI: 10.1103/PhysRevC.108.045501

I. INTRODUCTION

The standard model (SM) of particle physics in its original form [1–3] predicts massless neutrinos and is convincingly ruled out by neutrino oscillation experiments [4]. A minimal extension of the SM, called the νSM, adds two or more right-handed neutrinos, ν_R, which are singlets under the SM gauge groups and therefore called sterile neutrinos or, if their masses satisfy $M \gg \mathcal{O}(\text{eV})$, heavy neutral leptons [5]. At the renormalizable level, apart from a kinetic term, sterile neutrinos have a Majorana and a Dirac mass term connecting them to the SM left-handed lepton doublet and the Higgs field. Besides accommodating neutrino masses, this simple νSM has several intriguing features [6–11]. First of all, since a sterile neutrino Majorana mass term is not forbidden by symmetries, neutrinos generally become Majorana particles, leading to the violation of lepton number (LNV). Secondly, in the νSM it is possible to account for the baryon asymmetry of the universe [12]. Finally, a very light sterile neutrino can be a dark matter candidate [10,13–15].

Different experiments are sensitive to sterile neutrinos depending on their mass M. For all mass ranges, however, neutrinoless double-beta decay ($0\nu\beta\beta$) plays a prominent role. $0\nu\beta\beta$ is the most sensitive probe of LNV [16], with current limits on $0\nu\beta\beta$ half-lives exceeding 10^{26} yr [17,18] and prospects for improvements by two orders of magnitude in the next decade [19–25]. For $M \gg \mathcal{O}(\text{GeV})$, $0\nu\beta\beta$ decay is mainly driven by the exchange of light active neutrinos, and is proportional to the so-called effective neutrino mass $m_{\beta\beta}$. For lighter M there can be additional nonstandard contributions from the exchange of sterile neutrinos that can enhance or suppress the $0\nu\beta\beta$ rates. Contributions from sterile neutrinos to $0\nu\beta\beta$ have been studied extensively in the literature [26–36]. These works include the effect of the mass of the exchanged neutrinos by replacing the usual denominator of the massless neutrino propagator, $1/\mathbf{k}^2$, by a massive one, $1/(\mathbf{k}^2 + M^2)$, in the LNV potential used in nuclear many-body calculations. Here, we argue that this only captures one part of the M dependence in $0\nu\beta\beta$ amplitudes and that consistent computations should include additional terms that can significantly alter $0\nu\beta\beta$ rate predictions.

The paper is organized as follows. In Sec. II we establish the formalism for the calculation of the $0\nu\beta\beta$ half-life in the presence of active and sterile neutrinos, organizing different contributions according to the virtuality of the neutrinos that

*wdekens@uw.edu
†j.devries4@uva.nl
‡emereghetti@lanl.gov
§menendez@fqa.ub.edu
‖pablo-sf@hotmail.com
¶ghzhou@itp.ac.cn

mediate the $0\nu\beta\beta$ transition. In Sec. III we discuss the dependence of nuclear and hadronic matrix elements on the neutrino mass M and present a shell model calculation of the relevant nuclear matrix elements. In Sec. IV we analyze the impact of the new contributions identified in this paper on sterile neutrino phenomenology, before concluding in Sec. V.

II. NEUTRINOLESS DOUBLE β DECAY WITH ACTIVE AND STERILE NEUTRINOS

We consider a general setup with the SM Lagrangian supplemented by renormalizable interactions with n gauge-singlet neutrino fields

$$\mathcal{L} = \mathcal{L}_{SM} - \left[\frac{1}{2}\bar{\nu}_R^c M_R \nu_R + \bar{L}\tilde{H}Y_\nu \nu_R + \text{H.c.}\right], \tag{1}$$

in terms of the lepton doublet $L = (\nu_L,\, e_L)^T$, while $\tilde{H} = i\tau_2 H^*$ with H the Higgs doublet in the unitary gauge. ν_R is a column vector of n right-handed sterile neutrinos, Y_ν is a $3 \times n$ matrix of Yukawa couplings, and M_R is a symmetric $n \times n$ matrix. A Majorana mass term M_L for the left-handed neutrinos is forbidden by the gauge symmetry of the SM and it can only appear via nonrenormalizable operators of dimension greater than 4 [37].

After electroweak symmetry breaking, the neutrino mass term can be written as

$$\mathcal{L}_m = -\frac{1}{2}\bar{N}^c M_\nu N + \text{H.c.}, \quad M_\nu = \begin{pmatrix} 0 & M_D^* \\ M_D^\dagger & M_R^\dagger \end{pmatrix}, \tag{2}$$

where $N = (\nu_L,\, \nu_R^c)^T$ and $M_D = \frac{v}{\sqrt{2}}Y_\nu^\dagger$, with $v \simeq 246$ GeV. M_ν is a symmetric matrix diagonalized through

$$U^T M_\nu U = \text{diag}(m_1, \ldots, m_{3+n}), \quad N = UN_m. \tag{3}$$

U is the unitary neutrino mixing matrix, m_i are real and positive, and $\nu = N_m + N_m^c = \nu^c$. The active neutrino masses are light: $m_{1,2,3} \lesssim 1$ eV [38]. Because of the absence of M_L in Eq. (2), in the νSM

$$\sum_{i=1}^{n+3} U_{ei}^2 m_i = (M_\nu)_{ee}^* = 0, \tag{4}$$

which plays an important role for $0\nu\beta\beta$ [26,39].

Recent years have seen the development of a chiral effective field theory (χEFT) derivation of the so-called neutrino potential that induces $nn \to pp + ee$ transitions. χEFT provides an expansion in p/Λ_χ where the scales are given by the pion mass or nuclear Fermi momentum, $p \sim m_\pi \sim k_F = \mathcal{O}(100\,\text{MeV})$, and the breakdown scale, $\Lambda_\chi \sim 4\pi F_\pi \sim m_N = \mathcal{O}(1\,\text{GeV})$, in terms of the pion decay constant and the nucleon mass. χEFT was first applied to the construction of the $0\nu\beta\beta$ transition operators induced by higher-dimensional LNV operators in the standard model effective field theory (SMEFT) [40–43], assuming the standard "Weinberg's power counting" [44,45]. This approach was subsequently extended to the case of the exchange of light active Majorana neutrinos [46] and beyond Weinberg's counting [47,48]. Finally, the sterile-neutrino extension of the SMEFT (νSMEFT) was first addressed in Ref. [49].

In χEFT with active and sterile light neutrinos, the $0\nu\beta\beta$ rate receives contributions from exchanges of neutrinos, which can be systematically organized according to the scaling of the neutrino energy and momentum. In the case of light active Majorana-neutrino exchange, the leading order in the chiral expansion then arises from potential neutrinos, with momenta scaling as $k_0 \ll |\vec{k}| \sim k_F$, and hard neutrinos, scaling as $k_0 \sim |\vec{k}| \sim \Lambda_\chi$ [47,48]. Neutrinos with soft and ultrasoft momentum scalings come into play at next-to-next-to-leading order. The soft neutrinos, with momenta $k_0 \sim |\vec{k}| \sim m_\pi$, contribute through loop diagrams, while the momenta of ultrasoft neutrinos scale as $k_0 \sim |\vec{k}| \sim k_F^2/m_N$. The effects of all momentum regions can be described by a quantum mechanical Hamiltonian, see Eq. (10) of Ref. [46]. This Hamiltonian captures the effects of the potential, hard, and soft neutrinos in, generally nonlocal, LNV potentials, while the theory still contains ultrasoft modes as degrees of freedom.

In this section, we will extend this framework by considering minimal extensions of the SM in which the cancellation mechanism of Eq. (4) is active. This cancellation causes a suppression of the usually leading potential- and hard-neutrino exchange, which, depending on M, can lead to a relative enhancement of the contributions from soft or ultrasoft neutrinos. As described below, this results in a rearrangement of the power-counting discussed in Ref. [49], which continues to hold for sterile neutrinos with nonminimal interactions. Before discussing the νSM, we review the construction of the $0\nu\beta\beta$ operator in the case of active Majorana-neutrino exchange in Sec. II A, following closely the derivation of Refs. [46–48]. In Sec. II B, we then discuss the contribution of sterile neutrinos with arbitrary mass, but minimal interactions.

A. The $0\nu\beta\beta$ transition operator with active neutrinos

The exchange of light virtual Majorana neutrinos gives rise to a leading-order (LO) contribution from neutrinos with momenta $|\boldsymbol{k}| \sim k_F$ and $k_0 \sim |\boldsymbol{k}|^2/\Lambda_\chi$, defined as potential contributions. The order-by-order renormalizability of the $0\nu\beta\beta$ amplitude requires the promotion of an $nn \to pp + ee$ contact term to LO. This term captures contributions from hard neutrinos with momenta $k_0 \sim |\boldsymbol{k}| \sim \Lambda_\chi$ [47,48] and has been recently included in many-body computations [50–53]. The LO $0\nu\beta\beta$ half-life reads

$$\left(T_{1/2}^{0\nu}\right)^{-1} = G_{01}\, g_A^4 \left| \sum_{i=1}^{3} V_{ud}^2 \frac{U_{ei}^2 m_i}{m_e} A_\nu \right|^2, \tag{5}$$

and is factorized in a leptonic piece, the phase-space factor G_{01} ($G_{01} = 1.4 \times 10^{-14}\ \text{y}^{-1}$ for ^{136}Xe [54,55]), and a nuclear amplitude A_ν,

$$A_\nu = \frac{\mathcal{M}_F}{g_A^2} - \mathcal{M}_{GT} - \mathcal{M}_T - 2g_\nu^{NN} m_\pi^2 \frac{\mathcal{M}_{F,sd}}{g_A^2}, \tag{6}$$

where $g_A \simeq 1.27$ is the nucleon axial charge, $V_{ud} \simeq 0.97$ is the u-d element of the Cabibbo-Kobayashi-Maskawa (CKM) quark mixing matrix, $\mathcal{M}_F$, $\mathcal{M}_{GT}$, and $\mathcal{M}_T$ are the nuclear matrix elements (NMEs) of the Fermi, Gamow-Teller, and tensor long- and pion-range neutrino potentials, while $\mathcal{M}_{F,sd}$ is the

matrix element of the short-range contact term (see Ref. [16] for an overview). g_ν^{NN} is a low-energy constant (LEC) associated with hard-neutrino exchange that in principle can be calculated with lattice quantum chromodynamics (QCD) [56–59], but so far only phenomenological determinations are available [60–62].

Other contributions appear at next-to-next-to-leading order ($\mathrm{N^2LO}$). Here, we highlight a correction that plays an important role for sterile neutrinos. It arises from ultrasoft neutrinos with momentum scaling $k_0 \sim |\mathbf{k}| \sim k_F^2/m_N$ [46]. The ultrasoft amplitude is given by

$$A_\nu^{(\mathrm{usoft})}(m_i) = \frac{8\pi R_A}{g_A^2} \sum_n \langle 0_f^+|\mathcal{J}_\mu|n\rangle\langle n|\mathcal{J}^\mu|0_i^+\rangle \times \int \frac{d^{d-1}k}{(2\pi)^{d-1}} \frac{1}{E_\nu[E_\nu + \Delta E_1 - i\epsilon]} + (\Delta E_1 \to \Delta E_2), \tag{7}$$

where $E_\nu = \sqrt{\mathbf{k}^2 + m_i^2} \simeq |\mathbf{k}|$, $\Delta E_{1,2} = E_{1,2} + E_n - E_i$, with E_i and E_n denoting the energies of the initial and intermediate states, and $E_{1,2}$ stand for electron energies and $R_A \simeq 1.2\,A^{1/3}$ fm. $\mathcal{J}_\mu$ is the single nucleon charged current evaluated between the initial $|0_i^+\rangle$, final $|0_f^+\rangle$, and a complete set of intermediate states $|n\rangle$.

B. The $0\nu\beta\beta$ transition operator with sterile neutrinos

Previous works in the literature just combine the neutrino potential for light active neutrinos with a mass-dependent one for sterile neutrinos:

$$\sum_{i=1}^{3} \frac{U_{ei}^2 m_i}{\mathbf{k}^2} \to \sum_{i=1}^{3} \frac{U_{ei}^2 m_i}{\mathbf{k}^2} + \sum_{i=4}^{n+3} \frac{U_{ei}^2 m_i}{\mathbf{k}^2 + m_i^2} \tag{8}$$

for all values of m_i. In practice, this is done by computing $\mathcal{M}(m_i) = -(\mathcal{M}_F/g_A^2 - \mathcal{M}_{GT} - \mathcal{M}_T)(m_i)$ for a range of m_i and then fitting to the functional form [30,36,63–65]

$$\mathcal{M}(m_i) = \mathcal{M}(0)\frac{\langle p^2\rangle}{\langle p^2\rangle + m_i^2}, \tag{9}$$

where the exact value of $\langle p^2\rangle \sim k_F^2$ depends on the isotope and the applied nuclear many-body method. However, this approach does not include any other contributions, which leads to several shortcomings:

(i) NMEs become ill-defined for $m_i \gtrsim \Lambda_\chi$ because the χEFT expansion does not converge for $m_i/\Lambda_\chi \gtrsim 1$. These sterile neutrinos must be integrated out at the quark level leading to local dimension-9 operators which, after evolution to low-energy scales, can be matched to χEFT [49]. The resulting LECs and NMEs cannot be obtained from Eq. (9) because the dimension-9 operator does not factorize.

(ii) For $m_i \lesssim \Lambda_\chi$, Eq. (9) misses the LO contribution from hard neutrinos captured by the mass-dependent LEC, $g_\nu^{NN}(m_i)$.

(iii) If for all sterile neutrinos $m_i \ll k_F$, the $0\nu\beta\beta$ rate is suppressed because of Eq. (4) [26,39]. In this limit, Eq. (9) predicts

$$\left(T_{1/2}^{0\nu}\right)^{-1} = G_{01}\, g_A^4 \left| \sum_{i=1}^{n+3} V_{ud}^2 \frac{U_{ei}^2 m_i^3}{m_e\langle p^2\rangle} \mathcal{M}(0) \right|^2, \tag{10}$$

which is suppressed by $(m_i^2/\langle p^2\rangle)^2 \sim m_i^4/k_F^4$. However, ultrasoft contributions suffer a milder suppression of m_i^2/k_F^2 and $(\frac{m_i^2}{4\pi\,\Delta E\,k_F} \ln\frac{m_i}{\Delta E})^2$, where $\Delta E \sim k_F^2/m_N$ is a nuclear excitation energy. These effects lead to much faster decay rates.

We now discuss an improved description of the $0\nu\beta\beta$ amplitude for different regions of m_i.

1. Heavy masses: $m_i \gtrsim \Lambda_\chi$

Heavy sterile neutrinos can be integrated out at the quark level, giving rise to local operators containing four quarks and two electrons

$$\mathcal{L}^{(9)} = C_L(\mu_0)\bar{u}_L\gamma^\mu d_L \bar{u}_L\gamma_\mu d_L \bar{e}_L e_L^c \tag{11}$$

with $C_L(\mu_0) = -\eta(\mu_0, m_i)\frac{4V_{ud}^2 G_F^2}{m_i} U_{ei}^2$. $\eta(\mu_0, m_i)$ takes into account the QCD renormalization-group evolution from the scale m_i to $\mu_0 = 2$ GeV at which we match to χEFT. This evolution is mild and we include it into our results but we discuss it no further here. The matching to χEFT leads to hadronic LNV vertices [41,42,66] and a resulting amplitude

$$A_\nu^{(9)} = -2\eta(\mu_0, m_i)\frac{m_\pi^2}{m_i^2}\left[\frac{5}{6} g_1^{\pi\pi}\left(\mathcal{M}_{GT,sd}^{PP} + \mathcal{M}_{T,sd}^{PP}\right) + \frac{g_1^{\pi N}}{2}(\mathcal{M}_{GT,sd}^{AP} + \mathcal{M}_{T,sd}^{AP}) - \frac{2g_1^{NN}}{g_A^2}\mathcal{M}_{F,sd}\right], \tag{12}$$

where $g_1^{\pi\pi}$, $g_1^{N\pi}$, and g_1^{NN} are hadronic LECs. The $\mathcal{M}_i$ denote NMEs [66], which have been calculated for several nuclei [67–69]. In turn, $g_1^{\pi\pi}$ is currently the only LEC determined by lattice QCD [70–72]. Using the calculation of Ref. [70], we get $g_1^{\pi\pi} = 0.36(2)$ at the scale $\mu = 2$ GeV. The naive limit of Eq. (6) would yield the same expression as Eq. (12), but with $g_1^{\pi\pi} = 3/5$, $g_1^{\pi N} = 1$, and $g_1^{NN} = (1 + 3g_A^2)/4$. QCD effects thus cause $g_1^{\pi\pi}$ to differ by about a factor of 2 compared to the naive factorization approach. We expect similar deviations in $g_1^{\pi N}$ and g_1^{NN}, stressing the importance of controlling the hadronic input.

2. Intermediate masses: $k_F < m_i < \Lambda_\chi$

In this mass region, sterile neutrinos appear as explicit degrees of freedom in χEFT [49]. The potential contributions arise from Eq. (8), combined with the hard effects they give

$$A_\nu(m_i) = -\mathcal{M}(m_i) - 2g_\nu^{NN}(m_i)m_\pi^2\frac{\mathcal{M}_{F,sd}}{g_A^2}, \tag{13}$$

which requires knowledge of the m_i dependence of both the NMEs (from many-body calculations) and the LEC g_ν^{NN} (from nonperturbative QCD). In addition, there are contributions from loops involving soft sterile neutrinos, which for light neutrinos would contribute at $\mathrm{N^2LO}$ but here can give rise to terms scaling as m_i^2/Λ_χ^2. These effects lead to a breakdown of the χEFT expansion when $m_i \sim 1$ GeV. There are

no contributions from ultrasoft sterile neutrinos because the integral in Eq. (7) vanishes in dimensional regularization once the integrand is expanded in k/m_i.

3. Light masses: $m_i < k_F$

Here, the potential and hard regimes are similar as for active neutrinos. A new effect appears due to ultrasoft sterile neutrinos. When $k_F > m_i$, we can perform the integrals of Eq. (7),

$$A_\nu^{(\text{usoft})} = -\frac{R_A}{2\pi}\sum_n \langle 0^+|\tau^+\boldsymbol{\sigma}|n\rangle\langle n|\tau^+\boldsymbol{\sigma}|0^+\rangle \times [f(m_i, \Delta E_1) + f(m_i, \Delta E_2)]. \tag{14}$$

The function $f(m, E)$ can be computed analytically, giving

$$f(m,E) = \begin{cases} -2\left[E\left(1+\ln\frac{\mu_{us}}{m}\right) + \sqrt{m^2-E^2}\times\left(\frac{\pi}{2} - \tan^{-1}\frac{E}{\sqrt{m^2-E^2}}\right)\right] & m > E \\ -2\left[E\left(1+\ln\frac{\mu_{us}}{m}\right) - \sqrt{E^2-m^2}\ln\frac{E+\sqrt{E^2-m^2}}{m}\right] & m < E. \end{cases} \tag{15}$$

For $m_i \gg \Delta E$, f becomes independent of the energy splittings and approaches $f \sim -\pi m_i$, while, for $m_i \ll \Delta E$, $f \sim -\frac{m_i^2}{\Delta E}(\frac{1}{2} + \ln\frac{2\Delta E}{m_i})$. In both regions, the scaling with the sterile neutrino mass is more favorable than Eq. (10). In the region $m_i < \Delta E$, a similar logarithmic dependence was also found in Refs. [46,73]. The dependence on the ultrasoft renormalization scale, μ_{us}, cancels in the amplitude when taking into account soft loop corrections to the potential [46]. We therefore set $\mu_{us} = m_\pi$, which captures the log-enhanced part of the soft loops, and stress that the exact choice of μ_{us} does not impact the main result which is the modified m_i dependence of the amplitude.

III. NUCLEAR AND HADRON MATRIX ELEMENTS

The correct description of the $0\nu\beta\beta$ amplitude depends on several new NMEs and LECs. We calculate all necessary NMEs using the nuclear shell model, one of the leading many-body methods used for $\beta\beta$ decay [16,74]. We focus here on ^{136}Xe but our conclusions apply to other experimentally relevant isotopes, such as ^{76}Ge, as well. We use the GCN5082 effective Hamiltonian [75] in a configuration space comprising the $0g_{7/2}$, $1d_{5/2}$, $2s_{1/2}$, $1d_{3/2}$, and $0h_{11/2}$ single-particle orbitals for protons and neutrons. We obtain our results with the shell-model code NATHAN [76].

For potential contributions, we evaluate the explicit m_i dependence of the NME $\mathcal{M}_\nu(m_i) = -(\mathcal{M}_F/g_A^2 - \mathcal{M}_{GT} - \mathcal{M}_T)(m_i)$ of Eq. (6) in the range $5\,\text{MeV} < m_i < 2$ GeV. The numerical values are listed in Table I. A fit to Eq. (9) gives $\langle p^2\rangle \simeq (175\,\text{MeV})^2$. However, we use the functional form

$$\mathcal{M}(m_i) = \mathcal{M}(0)\frac{1}{1 + m_i/m_a + (m_i/m_b)^2}, \tag{16}$$

where $\mathcal{M}(0) = 2.7$, $m_a = 157$ MeV, and $m_b = 221$ MeV fit the calculated NMEs within a few-percent accuracy. Equation (16) contains a linear term in m_i different from the usually used functional form in Eq. (9). The data, together with the interpolation formula of Eq. (16), are shown in Fig. 1.

The ultrasoft contributions require the intermediate-state energies of ^{136}Cs, E_n, in addition to matrix elements involving also the ^{136}Xe and ^{136}Ba ground states. We use the Lanczos strength function method [76], which after several tens of iterations gives converged results for $A_\nu^{(\text{usoft})}$. Typical energy differences are $E_n - E_i \sim 1$–10 MeV, while the electron energies are $E_1 \simeq E_2 \simeq Q_{\beta\beta}/2 + m_e$ with $Q_{\beta\beta} \simeq 2.5$ MeV for ^{136}Xe, up to percent-level corrections of order $\mathcal{O}((E_2 - E_1)^2/(\Delta E_{1,2})^2)$. All computed NMEs, for 60 calculated intermediate states, are given in the Appendix.

The hard contributions depend on a hadronic and a nuclear matrix element: $\mathcal{M}_{F,\text{sd}} \times g_\nu^{NN}(m_i)$ which only in combination with $\mathcal{M}(m_i)$ is independent of the regulators used in nuclear computations [47]. The value of $g_\nu^{NN}(m_i)$ thus depends on the nuclear many-body method used. We follow Refs. [48,62,77] and connect $g_\nu^{NN}(0)$ to charge-independence-breaking nucleon-nucleon interactions, in good agreement

TABLE I. Shell-model $0\nu\beta\beta$ NMEs for ^{136}Xe as a function of the neutrino mass.

m_i (MeV)	$\mathcal{M}(m_i)$
5	2.6
6	2.6
7	2.6
8	2.6
9	2.6
10	2.5
20	2.4
30	2.3
40	2.1
50	2.0
60	1.9
70	1.8
80	1.7
90	1.6
100	1.5
200	0.94
300	0.61
400	0.42
500	0.32
600	0.23
700	0.18
800	0.14
900	0.11
1000	0.094
2000	0.025

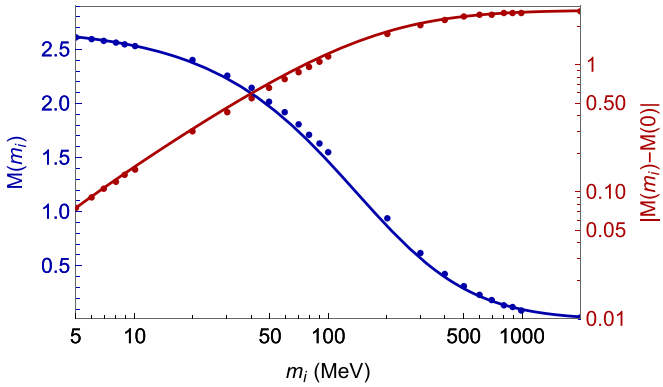

FIG. 1. NMEs in Eq. (6) for ^{136}Xe as a function of the neutrino mass (in blue), as well as the difference $\mathcal{M}(0) - \mathcal{M}(m_i)$ (in red). Circles indicate the numerical results of the shell-model calculations, while the solid lines depict the interpolation formula of Eq. (16).

with model estimates [60,61]. From the nuclear shell model we get $\mathcal{M}_{F,\mathrm{sd}} = -1.94$ for $g_\nu^{NN}(0) = -1.01\,\mathrm{fm}^2$ [77]. The m_i dependence is harder to pin down. Around $m_i \sim \Lambda_\chi$ the sum of the potential and hard contributions should match to Eq. (12) which requires $g_\nu^{NN}(m_i \sim \Lambda_\chi) \sim m_i^{-2}$. In the opposite limit, $m_i \ll k_F$, we have $g_\nu^{NN}(m_i) \simeq g_\nu^{NN}(0) + g_{\nu,2}^{NN} m_i^2$ with $g_{\nu,2}^{NN} = \mathcal{O}(f_\pi^{-2}\Lambda_\chi^{-2})$ from χEFT power counting. These scalings are obeyed by the functional form

$$g_\nu^{NN}(m_i) = g_\nu^{NN}(0)\frac{1 + (m_i/m_c)^2}{1 + (m_i/m_c)^2(m_i/m_d)^2}, \tag{17}$$

where $m_c = \mathcal{O}(\Lambda_\chi)$. Setting $m_c = 1$ GeV for concreteness we fix m_d by matching to Eq. (12) at $m_i = \mu_0$. To get a reasonable estimate we saturate $A_\nu^{(9)}$ with the $g_1^{\pi\pi}$ and g_1^{NN} contributions and set $g_1^{NN} \simeq (1 + 3g_A^2)/4$, the factorization estimate, and $g_1^{\pi\pi} = 0.36$ [70]. This recipe gives $m_d \simeq 146$ MeV and provides the most uncertain part of our analysis, which mostly affect the mass range $m_\pi - \Lambda_\chi$. For example, varying g_1^{NN} up and down by 50%, which affects m_d on a similar level, alters the total amplitude at $m_i = 500$ MeV by about 60%, while the effect below $m_i \leqslant m_\pi$ is negligible. The uncertainties in this description can be reduced by lattice QCD computations of all LECs in Eq. (12).

Finally, we connect the improved amplitude for different regions of m_i in the following way:

$$A_\nu(m_i) = \begin{cases} A_\nu^{(<)} + A_\nu^{(\mathrm{usoft})}, & m_i < 100\ \mathrm{MeV} \\ A_\nu, & 0.1\ \mathrm{GeV} \leqslant m_i < 2\ \mathrm{GeV}, \\ A_\nu^{(9)}, & 2\ \mathrm{GeV} \leqslant m_i \end{cases} \tag{18}$$

where $A_\nu^{(<)} = A_\nu + m_i \frac{d}{dm_i}\mathcal{M}(m_i)$. In the region $m_i < k_F$, Eq. (16) contains a linear term (after expanding) in m_i, not included in the standard functional form of Eq. (9). This linear term is dominated by ultrasoft contributions and, to avoid double counting between Eqs. (16) and (14), we remove it in the definition of $A_\nu^{(<)}$. The appearance of this linear term in $A_\nu^{(\mathrm{usoft})}$ and $\mathcal{M}$ allows for a consistency check, which we discuss in more detail in future work.

IV. PHENOMENOLOGY AND SPECIFIC MODELS

To illustrate the important effects of our findings, we consider two toy models that capture the essential features of realistic seesaw models with light sterile neutrinos.

A. The 3 + 1 scenario

We begin with the $3 + 1$ scenario with three light active neutrinos and one sterile neutrino. The 4×4 mass matrix has the following form:

$$M_\nu = \begin{pmatrix} 0 & M_{D,i}^* \\ M_{D,i}^* & |M_R| e^{i\alpha_R} \end{pmatrix}, \tag{19}$$

and we set $M_{D,1} = M_{D,2} = M_{D,3} \equiv |M_D| e^{i\alpha_D}$ for simplicity. The model leads to two massless neutrinos and is thus ruled out but illustrates the importance of ultrasoft corrections. Diagonalizing the mass matrix leads to one active neutrino mass, m_3, the sterile mass, m_4, and the mixing angles

$$U_{e3}^2 = -\frac{m_4}{m_3} U_{e4}^2 = -\frac{1}{3}\frac{m_4}{m_3 + m_4} e^{i(2\alpha_D + \alpha_R)}, \tag{20}$$

where $\alpha_{D,R}$ drop out in the $0\nu\beta\beta$ rate.

We set $m_3 \simeq 0.05$ eV and show the resulting half-life of ^{136}Xe in Fig. 2. In the light m_4 regime, the lifetimes obtained from our approach (solid black) are much shorter than those obtained from Eq. (9) (roughly three orders of magnitude for $m_4 = 10$ MeV) because of the ultrasoft contributions. The enhancement for $m_4 > 100$ MeV is smaller, about a factor of 2, and mainly caused by hard-neutrino contributions. Such an enhancement is also found for light active neutrinos [47,50,77].

B. The pseudo-Dirac scenario

The masses of active neutrinos discussed above are inversely proportional to the Majorana mass of the sterile neutrino. This causes small mixing angles and thus very long lifetimes, in particular in the regime where $m_4 < 100$ MeV. Much larger mixing angles are possible in inverse seesaw models [78–80] in which the active and sterile Majorana masses become proportional to a small LNV parameter, leading to pseudo-Dirac sterile neutrinos. Variants of these models appear in scenarios of low-scale leptogenesis which have been intensively developed in recent years, see, e.g., Refs. [8,81,82]. While a full model contains many parameters and requires a dedicated scan, here, we focus on a simplified case that captures the salient features of the inverse seesaw model. We show that with our new contributions, next-generation $0\nu\beta\beta$ experiments can set the most stringent limits, or make the first detection, in a large part of the sterile neutrino mass range.

We consider the inverse seesaw $1 + 2$ scenario [78–80] with one active and two sterile neutrinos. The 3×3 mass matrix has the form

$$M_\nu = \begin{pmatrix} 0 & m_D & 0 \\ m_D & \mu_X & m_S \\ 0 & m_S & \mu_S \end{pmatrix}. \tag{21}$$

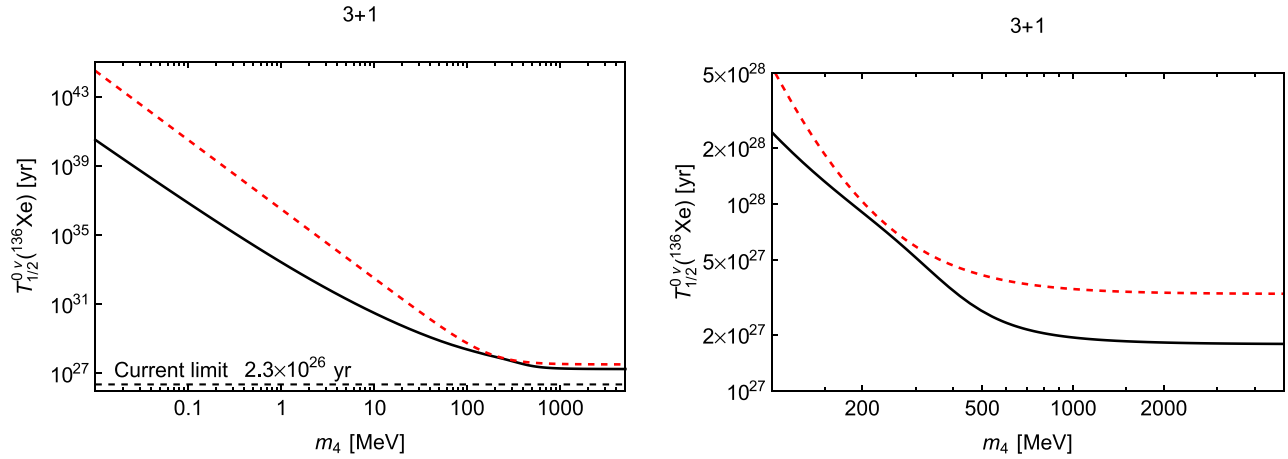

FIG. 2. $0\nu\beta\beta$ half-life of ^{136}Xe as a function of m_4 in the $3+1$ model, obtained with the NMEs in Eqs. (9) (dashed red) and (18) (black). The right panel focuses on the results for larger m_4 values.

Together with the assumption $m_S \gg m_D$, $\mu_{X,S}$, the mass of the lightest neutrino satisfies $m_\nu \simeq -(m_D^2\mu_S)/m_S^2$ and is proportional to the small LNV parameter, μ_S. We set $m_\nu = 2.6 \times 10^{-3}$ eV (as a typical value of $m_{\beta\beta}$ in the normal hierarchy) and write $M_{1,2}$ for the masses of the heavier neutrinos. We focus on a scenario where the heavier states act as a pseudo-Dirac pair with a small mass splitting. The mass matrix in this model can be diagonalized by

$$U = \begin{pmatrix} 1 & 0 & 0 \\ 0 & c_{12} & s_{12} \\ 0 & -s_{12} & c_{12} \end{pmatrix} \cdot \begin{pmatrix} c_{e2} & 0 & s_{e2}e^{-i\delta} \\ 0 & 1 & 0 \\ -s_{e2}e^{i\delta} & 0 & c_{e2} \end{pmatrix} \cdot \begin{pmatrix} c_{e1} & s_{e1} & 0 \\ -s_{e1} & c_{e1} & 0 \\ 0 & 0 & 1 \end{pmatrix} \cdot \begin{pmatrix} 1 & 0 & 0 \\ 0 & e^{i\alpha_1} & 0 \\ 0 & 0 & e^{i(\alpha_2+\delta)} \end{pmatrix}, \tag{22}$$

where $s_{ij} = \sin\theta_{ij}$ and $c_{ij} = \cos\theta_{ij}$. Setting $\alpha_1 = 0$ and $\alpha_2 = \pi/2$ allows the sterile neutrinos to act as a pseudo-Dirac pair. This choice, together with the constraint $(M_\nu)_{11} = 0$, then allows one to write the $0\nu\beta\beta$ rate in terms of the neutrino masses and $|U_{eN_1}|^2 + |U_{eN_2}|^2$.

The current limit on the half-life of ^{136}Xe [17] constrains the effective active-sterile mixing angle $|U_{eN_1}|^2 + |U_{eN_2}|^2$ [note that $|U_{eN_1}|^2 \approx |U_{eN_2}|^2$ up to $\mathcal{O}(\Delta/M_2)$ corrections where $\Delta = M_2 - M_1$]. Figure 3 shows these limits as a function of M_2 for $\Delta/M_2 = 1\%$. Limits for smaller (larger) splittings weaken (strengthen) as Δ^{-1}. The black line denotes limits obtained by using the results of this work which are compared to literature approaches [through Eq. (9)] shown in red. Finally, the gray region depicts parts of the parameter space where $3|\Delta| \leqslant |(M_\nu)_{22}|$, in tension with the pseudo-Dirac assumption, $\mu_X \sim \Delta$.This gray region can be obtained by using the constraint $(M_\nu)_{13} = 0$.

As in the $3+1$ model, the ultrasoft terms lead to significantly tighter constraints on the mixing angles for $M_2 < 100$ MeV. The $0\nu\beta\beta$ constraints are suppressed by the small mass splitting but nevertheless are competitive with other limits (indicated in purple and obtained from Refs. [63,83]) for masses lighter than a few hundred MeV. In particular, for this choice of parameters, the tonne-scale experiments will yield very competitive, if not the most stringent, bounds for masses between 1 and 100 MeV. In this region, currently the best limits come from pion decay, $\pi \to e\nu$ [84], and from the production of a sterile neutrino in the decay of ^{8}B, measured by Borexino [85]. Even with the proposed PIONEER experiment [86], which will improve the bounds from pion decay by a factor of ten on approximately the same timescale as the next generation tonne-scale experiments, $0\nu\beta\beta$ will remain very competitive in the 10–100 MeV regions. With the decommissioning of Borexino, we are not aware of upcoming improvements in the 1–10 MeV region. For heavier masses, the hard neutrino-exchange contributions again lead to

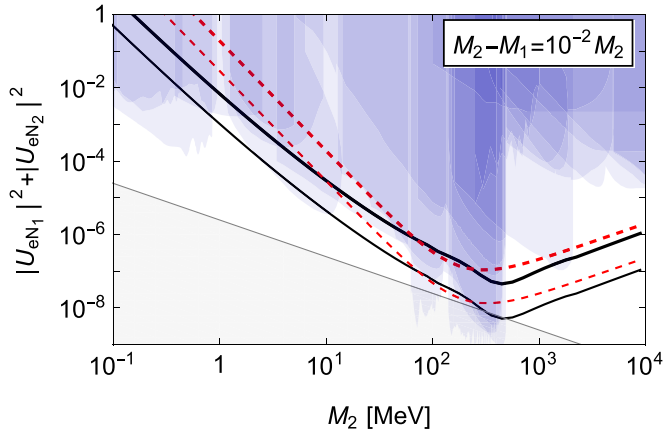

FIG. 3. Limit on the mixing angles, $|U_{eN_1}|^2 + |U_{eN_2}|^2$, as a function of M_2 in the pseudo-Dirac scenario for a mass splitting $\frac{M_2-M_1}{M_2} = 10^{-2}$. The black line corresponds to the $0\nu\beta\beta$ rate obtained in this work, whereas the red dashed line is based on Eq. (9). The thick and thin lines correspond to the current limit [17] and projected constraints at the level of $T^{0\nu}_{1/2} < 10^{28}$ yr, respectively. The blue background depicts other experiments [63,83], while the gray region indicates parameter space inconsistent within the assumptions of the model.

TABLE II. One-body matrix elements relevant for ultrasoft neutrino contributions to the $0\nu\beta\beta$ of ^{136}Xe.

$\frac{E_n-E_i}{\text{MeV}}$	$\langle n\|\boldsymbol{\sigma}\tau^+\|0_i^+\rangle$	$\langle 0_f^+\|\boldsymbol{\sigma}\tau^+\|n\rangle$
0.17	1.0	0.13
0.63	−0.19	−0.0063
0.89	−0.25	−0.016
1.02	0.30	0.036
1.05	0.23	0.025
1.1	−0.13	−0.00076
1.2	0.12	−0.0052
1.3	0.16	−0.0028
1.4	−0.23	−0.0098
1.5	0.20	−0.012
1.6	−0.36	0.0084
1.7	−0.24	0.00058
1.9	0.22	0.011
2.0	0.34	0.0070
2.2	0.35	0.0060
2.3	−0.49	−0.0086
2.6	0.62	0.021
2.7	−0.91	−0.024
2.9	0.37	0.0064
3.1	0.30	0.0013
3.3	0.39	−0.0013
3.6	0.39	0.0021
3.8	0.45	−0.013
4.0	−0.44	−0.0032
4.3	−0.35	−0.0038
4.6	−0.36	−0.0067
4.8	0.44	0.0083
5.1	0.44	0.0066
5.4	−0.55	−0.0093
5.7	0.63	0.012
6.1	0.85	0.013
6.3	−1.2	−0.016
6.7	−1.3	−0.014
7.0	−1.9	−0.016
7.3	3.1	0.023
7.5	−4.0	−0.028
7.7	2.6	0.017
8.1	1.4	0.0091
8.4	−1.0	−0.0057
8.8	−0.93	−0.0064
9.1	0.80	0.0038
9.4	0.59	0.0014
9.8	−0.50	0.0027
10.1	0.35	−0.0027
10.5	0.26	−0.00053
10.9	−0.22	−0.00021
11.3	0.17	−0.00037
11.7	−0.16	−0.00054
12.0	−0.16	−0.0010
12.4	0.14	0.00092
12.8	0.12	−0.00014
13.1	0.092	−0.00040
13.5	−0.079	−0.00019
13.9	0.071	−0.00026
14.2	−0.070	0.000031
14.6	−0.035	0.00021
15.1	−0.051	−0.00015
16.2	−0.039	0.00011
17.3	−0.043	−0.000091
17.7	0.11	−0.000029

somewhat tighter limits (a factor 2.5 for $m_i \simeq 400$ MeV) than obtained from Eq. (9) and are significantly stronger than other constraints despite the small mass splitting. Next-generation $0\nu\beta\beta$ experiments will probe uncharted parameter space over a large fraction of the mass range, even in the MeV range because of the ultrasoft contributions identified in this work.

V. CONCLUSIONS AND OUTLOOK

We have performed a systematic EFT derivation of the $0\nu\beta\beta$ rate in the neutrino-extended standard model, allowing us to identify and calculate novel contributions to $0\nu\beta\beta$. The largest correction can enhance the decay rate by orders of magnitude and arises from the exchange of light, ultrasoft neutrinos which induce a sterile neutrino mass dependence of the $0\nu\beta\beta$ amplitude that differs from previous studies in the literature. We also find new contributions associated with the exchange of light, hard neutrinos, which can lead to differences compared to known expressions by a factor of a few. Thus, these new effects can significantly enhance the $0\nu\beta\beta$ rates in neutrino-mass models of interest.

Looking to the future, our expressions can be made more accurate by first-principle determinations of various QCD matrix elements associated with virtual Majorana neutrino exchange. Lattice QCD calculations of such matrix elements are already underway for active (and thus essentially massless) neutrino exchange [57] and can be extended to massive neutrino exchange as well [87]. The expressions obtained in this work can be directly used to determine $0\nu\beta\beta$ rates in realistic minimal neutrino extensions that can resolve shortcomings of the SM such as the neutrino-mass mechanism, leptogenesis, and dark matter.

ACKNOWLEDGMENTS

We thank Bhupal Dev for discussions on the results of Refs. [63,83] and Cliff Burgess for useful comments. W.D. acknowledges support by the U.S. DOE under Grant No. DE-FG02-00ER41132. J.dV. acknowledges support from the Dutch Research Council (NWO) in the form of a VIDI grant. This work was supported by the "Ramón y Cajal" program with Grant No. RYC-2017-22781, and Grants No. CEX2019-000918-M and PID2020-118758GB-I00 funded by MCIN/AEI/10.13039/501100011033, by "ESF Investing in your future". E.M. was supported by the U.S. Department of Energy through the Los Alamos National Laboratory and by the Laboratory Directed Research and Development program of Los Alamos National Laboratory under Project No. 20230047DR. Los Alamos National Laboratory is operated by Triad National Security, LLC, for the National Nuclear Security Administration of U.S. Department of Energy (Contract No. 89233218CNA000001).

APPENDIX: NUCLEAR MATRIX ELEMENTS

Table I lists the numerical values of the NME, $\mathcal{M}_\nu(m_i) = -(\mathcal{M}_F/g_A^2 - \mathcal{M}_{GT} - \mathcal{M}_T)(m_i)$ of Eq. (6), as a function of the neutrino mass. The data, together with the interpolation formula of Eq. (16), are shown in Fig. 1. Table II provides the difference between initial and intermediate states and the Gamow-Teller matrix elements needed for the evaluation of the ultrasoft contribution.

[1] S. L. Glashow, Nucl. Phys. **10**, 107 (1959).
[2] A. Salam and J. C. Ward, Nuovo. Cim. **11**, 568 (1959).
[3] S. Weinberg, Phys. Rev. Lett. **19**, 1264 (1967).
[4] R. L. Workman *et al.* (Particle Data Group), PTEP **2022**, 083C01 (2022).
[5] A. M. Abdullahi *et al.*, J. Phys. G: Nucl. Part. Phys. **50**, 020501 (2023).
[6] T. Asaka, M. Shaposhnikov, and A. Kusenko, Phys. Lett. B **638**, 401 (2006).
[7] M. Shaposhnikov, J. High Energy Phys. 08 (2008) 008.
[8] L. Canetti, M. Drewes, T. Frossard, and M. Shaposhnikov, Phys. Rev. D **87**, 093006 (2013).
[9] M. Drewes, B. Garbrecht, P. Hernandez, M. Kekic, J. Lopez-Pavon, J. Racker, N. Rius, J. Salvado, and D. Teresi, Int. J. Mod. Phys. A **33**, 1842002 (2018).
[10] A. Boyarsky, M. Drewes, T. Lasserre, S. Mertens, and O. Ruchayskiy, Prog. Part. Nucl. Phys. **104**, 1 (2019).
[11] B. Dasgupta and J. Kopp, Phys. Rep. **928**, 1 (2021).
[12] S. Davidson, E. Nardi, and Y. Nir, Phys. Rep. **466**, 105 (2008).
[13] M. Drewes, Int. J. Mod. Phys. E **22**, 1330019 (2013).
[14] A. Kusenko, Phys. Rep. **481**, 1 (2009).
[15] M. Drewes *et al.*, J. Cosmol. Astropart. Phys. 01 (2017) 025.
[16] M. Agostini, G. Benato, J. A. Detwiler, J. Menéndez, and F. Vissani, Rev. Mod. Phys. **95**, 025002 (2023).
[17] S. Abe *et al.* (KamLAND-Zen Collaboration), Phys. Rev. Lett. **130**, 051801 (2023).
[18] M. Agostini *et al.* (GERDA Collaboration), Phys. Rev. Lett. **125**, 252502 (2020).
[19] N. Abgrall *et al.* (LEGEND Collaboration), arXiv:2107.11462 [nucl-ex]
[20] G. Adhikari *et al.* (nEXO Collaboration), J. Phys. G: Nucl. Part. Phys. **49**, 015104 (2022).
[21] C. Augier *et al.* (CUPID-Mo Collaboration), Eur. Phys. J. C **82**, 1033 (2022).
[22] D. Q. Adams *et al.* (NEXT Collaboration), J. High Energy Phys. 07 (2021) 164.
[23] V. Albanese *et al.* (SNO+ Collaboration), J. Inst. **16**, P08059 (2021).
[24] F. Agostini *et al.* (DARWIN Collaboration), Eur. Phys. J. C **80**, 808 (2020).
[25] C. Adams *et al.*, arXiv:2212.11099 [nucl-ex].
[26] M. Blennow, E. Fernandez-Martinez, J. Lopez-Pavon, and J. Menéndez, J. High Energy Phys. 07 (2010) 096.
[27] M. Mitra, G. Senjanović, and F. Vissani, Nucl. Phys. B **856**, 26 (2012).
[28] Y. F. Li and S.-s. Liu, Phys. Lett. B **706**, 406 (2012).
[29] A. de Gouvêa and W.-C. Huang, Phys. Rev. D **85**, 053006 (2012).
[30] A. Faessler, M. González, S. Kovalenko, and F. Šimkovic, Phys. Rev. D **90**, 096010 (2014).
[31] J. Barea, J. Kotila, and F. Iachello, Phys. Rev. D **92**, 093001 (2015).
[32] C. Giunti and E. M. Zavanin, J. High Energy Phys. 07 (2015) 171.
[33] T. Asaka and M. Shaposhnikov, Phys. Lett. B **620**, 17 (2005).
[34] T. Asaka, S. Eijima, and H. Ishida, J. High Energy Phys. 04 (2011) 011.
[35] T. Asaka and S. Eijima, PTEP **2013**, 113B02 (2013).
[36] T. Asaka, S. Eijima, and H. Ishida, Phys. Lett. B **762**, 371 (2016).
[37] S. Weinberg, Phys. Rev. Lett. **43**, 1566 (1979).
[38] M. Aker *et al.* (KATRIN Collaboration), Nat. Phys. **18**, 160 (2022).
[39] A. de Gouvêa, Phys. Rev. D **72**, 033005 (2005).
[40] M. J. Savage, Phys. Rev. C **59**, 2293 (1999).
[41] G. Prézeau, M. Ramsey-Musolf, and P. Vogel, Phys. Rev. D **68**, 034016 (2003).
[42] M. L. Graesser, J. High Energy Phys. 08 (2017) 099.
[43] V. Cirigliano, W. Dekens, J. de Vries, M. L. Graesser, and E. Mereghetti, J. High Energy Phys. 12 (2017) 082.
[44] S. Weinberg, Phys. Lett. B **251**, 288 (1990).
[45] S. Weinberg, Nucl. Phys. B **363**, 3 (1991).
[46] V. Cirigliano, W. Dekens, E. Mereghetti, and A. Walker-Loud, Phys. Rev. C **97**, 065501 (2018).
[47] V. Cirigliano, W. Dekens, J. de Vries, M. L. Graesser, E. Mereghetti, S. Pastore, and U. Van Kolck, Phys. Rev. Lett. **120**, 202001 (2018).
[48] V. Cirigliano, W. Dekens, J. de Vries, M. L. Graesser, E. Mereghetti, S. Pastore, M. Piarulli, U. van Kolck, and R. B. Wiringa, Phys. Rev. C **100**, 055504 (2019).
[49] W. Dekens, J. de Vries, K. Fuyuto, E. Mereghetti, and G. Zhou, J. High Energy Phys. 06 (2020) 097.
[50] R. Wirth, J. M. Yao, and H. Hergert, Phys. Rev. Lett. **127**, 242502 (2021).
[51] R. Weiss, P. Soriano, A. Lovato, J. Menéndez, and R. B. Wiringa, Phys. Rev. C **106**, 065501 (2022).
[52] A. Belley *et al.*, arXiv:2308.15634 [nucl-th].
[53] A. Belley, T. Miyagi, S. R. Stroberg, and J. D. Holt, arXiv:2307.15156 [nucl-th].
[54] A. Neacsu and M. Horoi, Adv. High Energy Phys. (2016) 7486712.
[55] J. Kotila and F. Iachello, Phys. Rev. C **85**, 034316 (2012).
[56] V. Cirigliano *et al.*, J. Phys. G: Nucl. Part. Phys. **49**, 120502 (2022).
[57] Z. Davoudi and S. V. Kadam, Phys. Rev. Lett. **126**, 152003 (2021).
[58] V. Cirigliano, W. Detmold, A. Nicholson, and P. Shanahan, Prog. Part. Nucl. Phys. **112**, 103771 (2020).
[59] Z. Davoudi and S. V. Kadam, Phys. Rev. D **105**, 094502 (2022).
[60] V. Cirigliano, W. Dekens, J. de Vries, M. Hoferichter, and E. Mereghetti, J. High Energy Phys. 05 (2021) 289.
[61] V. Cirigliano, W. Dekens, J. de Vries, M. Hoferichter, and E. Mereghetti, Phys. Rev. Lett. **126**, 172002 (2021).

[62] T. R. Richardson, M. R. Schindler, S. Pastore, and R. P. Springer, Phys. Rev. C **103**, 055501 (2021).
[63] P. D. Bolton, F. F. Deppisch, and P. S. Bhupal Dev, J. High Energy Phys. 03 (2020) 170.
[64] D.-L. Fang, Y.-F. Li, and Y.-Y. Zhang, Phys. Lett. B **833**, 137346 (2022).
[65] P. D. Bolton, F. F. Deppisch, M. Rai, and Z. Zhang, arXiv:2212.14690 [hep-ph].
[66] V. Cirigliano, W. Dekens, J. de Vries, M. L. Graesser, and E. Mereghetti, J. High Energy Phys. 12 (2018) 097.
[67] J. Hyvärinen and J. Suhonen, Phys. Rev. C **91**, 024613 (2015).
[68] J. Menéndez, J. Phys. G: Nucl. Part. Phys. **45**, 014003 (2018).
[69] J. Barea, J. Kotila, and F. Iachello, Phys. Rev. C **91**, 034304 (2015).
[70] A. Nicholson *et al.*, Phys. Rev. Lett. **121**, 172501 (2018).
[71] W. Detmold and D. Murphy (NPLQCD Collaboration), arXiv:2004.07404 [hep-lat].
[72] W. Detmold, W. I. Jay, D. J. Murphy, P. R. Oare, and P. E. Shanahan, Phys. Rev. D **107**, 094501 (2023).
[73] P. Bamert, C. P. Burgess, and R. N. Mohapatra, Nucl. Phys. B **438**, 3 (1995).
[74] J. Engel and J. Menéndez, Rep. Prog. Phys. **80**, 046301 (2017).
[75] E. Caurier, F. Nowacki, A. Poves, and K. Sieja, Phys. Rev. C **82**, 064304 (2010).
[76] E. Caurier, G. Martinez-Pinedo, F. Nowacki, A. Poves, and A. P. Zuker, Rev. Mod. Phys. **77**, 427 (2005).
[77] L. Jokiniemi, P. Soriano, and J. Menéndez, Phys. Lett. B **823**, 136720 (2021).
[78] R. N. Mohapatra and J. W. F. Valle, Phys. Rev. D **34**, 1642 (1986).
[79] R. N. Mohapatra, Phys. Rev. Lett. **56**, 561 (1986).
[80] S. Nandi and U. Sarkar, Phys. Rev. Lett. **56**, 564 (1986).
[81] M. Drewes, Y. Georis, and J. Klarić, Phys. Rev. Lett. **128**, 051801 (2022).
[82] P. Hernández, J. Lopez-Pavon, N. Rius, and S. Sandner, J. High Energy Phys. 12 (2022) 012.
[83] P. D. Bolton, P. S. Bhupal Dev, and F. F. Deppisch, https://www.hep.ucl.ac.uk/~pbolton/index.html#.
[84] M. Aoki *et al.* (PIENU Collaboration), Phys. Rev. D **84**, 052002 (2011).
[85] G. Bellini *et al.* (Borexino Collaboration), Phys. Rev. D **88**, 072010 (2013).
[86] W. Altmannshofer *et al.* (PIONEER Collaboration), arXiv:2203.01981 [hep-ex].
[87] X.-Y. Tuo, X. Feng, and L.-C. Jin, Phys. Rev. D **106**, 074510 (2022).